STRAIN INDUCED PHASE TRANSFORMATION IN Ti-15Mo β ALLOY

Xiaoming Wang[a] and Bernard Li[b]

[a]School of Engineering Technology, Purdue University, West Lafayette, IN47906, USA

[b]Medtronic Neuromodulation, 7000 Central Avenue NE, Minneapolis, MN55432 USA

Keywords: β-Titanium, Ti-Mo alloy, Strain induced phase transformation

Abstract

β-Ti alloys have been chosen for biomedical applications attributed to a combination of high strength, high fatigue resistance, good corrosion resistance and more importantly low modulus closer than other metallic materials for implants and osseointegrated prosthesis to the cortical elastic modulus (4-30 GPa). However, the phase constituents and phase transformation are still under dispute. A Ti-15Mo alloy after severe cold plastic deformation is studied to reveal the phases and phase transformation by TEM techniques. Athermal ω phase was observed in all samples evidencing the high stability of ω phase compared to β phase. However, the β to ω transformation does not proceed to a completion in heat treatment. Strain induced phase transformation happens in cold-draw wires through a coordinated shuffle of atoms along the {2 1 1}planes of β phase leading to the reduction on the <1 1 1> directions. The atomic level of shear causes the transformation of β to ω. The transformation of β to athermal ω under a train is not in a stable state but having a variable crystal structure between β and ω.

Introduction

β-Ti alloys have been chosen for biomedical applications attributed to a combination of high strength, high fatigue resistance, good corrosion resistance and more importantly low modulus closer than other metallic materials for implants and osseointegrated prosthesis to the cortical elastic modulus (4-30 GPa) [1-6]. β-Ti alloys are also a group of important structural materials for aeronautical applications due to lightweight, high strength and ductility, and additionally good workability [7-10]. The excellent corrosion resistance of β-Ti alloys makes the alloys suitable for applications in a corrosive environment, such as downhole oil drilling/exploration equipment [7, 11, 12]. The mechanical properties of β-Ti alloys can be tailored in a broad range through microstructural control for different applications, i.e. UTS from 690 MPa to 1586 MPa, modulus from 55 GPa to 110 GPa, elongation up to 17% and pseudoelasticity [2, 4, 7, 13-18]. However, β-Ti phase has a body-centered cubic (BCC) crystal structure and is not thermodynamic stable at room temperature. It is preserved by the addition of alloying elements called β-phase stabilizers [7]. The metastable nature of the β-Ti phase has caused a lot of confusion about the phase transformation of β-Ti alloys in processing, particularly in cold working/annealing, and therefore about the strengthening mechanisms under different conditions [19-25]. The phase transformation of β-Ti to α-Ti through a series of β + β′ and ω, α′ or α″ etc. is further complicated by a recently reported O′ metastable phase [26-30].

The β->α phase transformation is realized through slow cooling from the β phase or aging below the β transus with a certain crystal orientation relationship (OR) between the hexagonal close packed (HCP) α and the parental BCC β phase to reach a thermodynamic stable α phase [31, 32]. Meanwhile, metastable ω, α′ or α″ and O′ phases can form during the β to α transformation [19, 20, 29, 33, 34]. Both athermal and isothermal ω phase with the same hexagonal crystal structure can precipitate from the parent β phase. The athermal ω phase forms during β quenching, whereas the isothermal ω phase forms during ageing at temperatures below 823 K [13]. It appears as small (nanoscaled) cuboidal or ellipsoidal particles with a specific OR with the β matrix [20]. The two kinds of martensite, α′ (hexagonal) and α″ (orthorhombic) phases with an acicular or a plate shape form during rapid cooling from a temperature above or near β transus. The solute-depleted β and the solute-enriched β′ phases appear concomitantly with a rod-like morphology and are formed through spinodal decomposition at the early stage of low-temperature ageing. The structure of the two β products are BCC, as same as the parent β phase, resulting in no extra diffraction spots other than those of β in a selected area electron diffraction (SAED) pattern [35]. The phase transformation is further complicated by the fact that α to ω and β to ω transformation are enhanced by stress, resulting in combined phase transformation induced plasticity (TRIP) and twinning induced plasticity (TWIP) [21, 22, 36-38].

This paper presents findings on the phase transformation of a Ti-15Mo alloy after severe cold working in comparison with different heat treatment processes. An effort has been made on understanding the evolution of phases in severe cold working β-Ti alloy in relationship to its special properties, pseudoelasticity and a combination of high strength and low modulus.

Materials and Experiments

A Ti-15Mo β-alloy has been selected for the study to understand the phase transformation in both heat treatment and cold working due to its simplicity in terms of compositional variables. Ti-15Mo rods with a 5 mm diameter that have been solutionized at 740^{o}C for 20 minutes and then quenched in water were chosen as the raw material. For heat treatment, the rods were solutionized at 900^{o}C for 2 hours and cooled to room temperature at different cooling rates from 1^{o}C/s to 1000^{o}C/s. The rods were also cold drawn to an 80 micrometers diameter under room temperature for microstructural analysis. The microstructure of the rods is presented in Fig. 1 for comparison with the heat-treated and cold drawn microstructures in the following Results section.

Both original and heat treated rods were cut and polished for microstructural analysis following a standard metallographic procedure. The SEM images were taken by using an FEI 3D Quanta Dual Beam SEM operated at 20 kV. A Philips XL-40 microscope with EBSD capability was operated at 30 kV acceleration voltage and a working distance of 10 mm for EBSD and SEM images. Discs of 3 mm diameter were also punched from thin discs perpendicular to the axis of the rods and electropolished to perforation in a Tenupol ElectropolisherTM at –35^{o}C and 70 volts, using the following reagent: 4% perchloric acid, 2% hydrochloric acid, 36% butyl alcohol and 58% methanol. Helios 600i dual-column focused ion beam (FIB)/field emission scanning electron microscope (FESEM) operated at 30 kV was used for taking thin films for transmission electron microcopy from the wires and rods. Transmission electron microscopy (TEM) was done on an FEI Talos 200 X operated at 200 kV.

Results and discussions

A typical TEM image of the original rods is presented in Fig. 1(a) with a selected area diffraction (SAD) pattern as an insert. The typical microstructure is characterized by well-defined β-phase grains of about 1 μm diameter. The grains are not perfect crystalline with defects as shown by the contrasts in the image. There are also smaller Mo-depleted grains (called Mo-depleted particles in the following) forming along the normal β grain boundaries. An example of the particles is shown in Fig. 1 (b) with a corresponding EDX mapping of Mo element (Fig. 1 (c)). The SAD pattern in Fig. 1 (a) revealed the existence of ω-phase in a β-phase matrix. There were no other phases identified by electron diffraction. The matrix and the Mo-depleted particles are likely β and β′, which are formed through a bimodal chemical decomposition of the matrix β-phase [26-28]. The formation of Mo-enriched β-phase and Mo-depleted β′-phase were reported in β titanium. There are no information about the differences in mechanical properties of the two β phases. Therefore, their effects on the follow on cold processing will not be discussed separately.

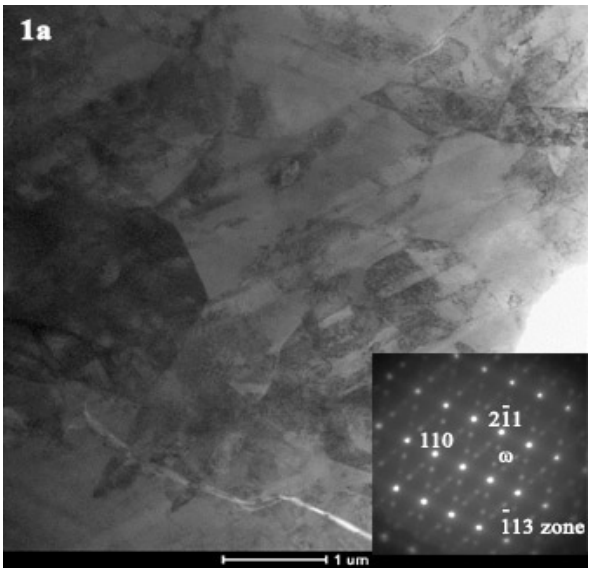
1a
$2\bar{1}1$
110
ω
$\bar{1}13$ zone
1 um

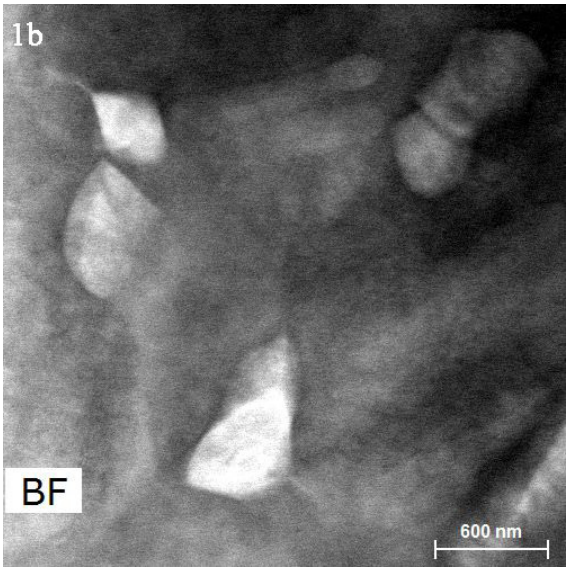
1b
BF
600 nm

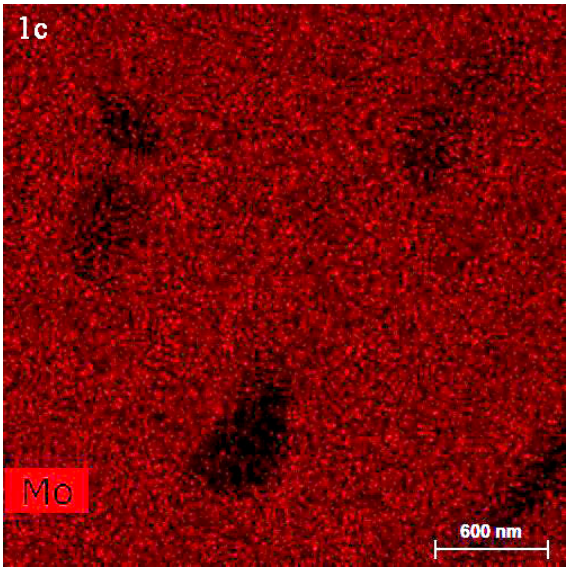

Fig. 1, (a) TEM bright field image of the original rods (Insert is a β -113 zone SAD pattern showing both β and ω phases), (b) Mo-depleted particles in originall rods and (c) EDX elemental mapping of Mo

Severe plastic deformation, cold drawing in this study, of the rods resulted in a microstructure that is shown in Figs. 2 (a)-(c). At a lower magnification, sharp contrasts appear due to highly localized strains, a common cold drawn feature. Traces of material flow can be seen resulting in crystal imperfections and therefore high contrasts. The traces are parallel to the longitudinal direction of the wire, i.e. the drawing direction. Images that were taken perpendicular to the wire show irregular shape contours of severely deformed regions. The deformation in cold drawing is not uniform at a micrometer level.

A high magnification image in Fig. 2 (c) revealed the existence of platelets of nanometers thickness parallel to the drawing direction. The platelets are a few hundred nanometers in length and about 50 nanometers in width. Further analysis revealed the modulation nature of the platelets, i.e. there is not a clear crystal orientation change across the platelet boundaries. This is different from the reported deformation twins by others, where further deformation is localized in small size twins [28]. The strengthening effects of nano twins have been well documented attributed to their effects on the emission and deflection of dislocations and back-stress thus generated [39]. In comparison,

the platelets of less than 100 nm thickness in Fig. 2 (c) result in the aforementioned special properties of the β Ti-15Mo alloy. Deformation heterogeneity is also clear from the image where a large size plate exists most likely due to its higher hardness than its surrounding β-phase grains, which could be an evidence of different hardness of the β and β′ phases. Furthermore, no dynamic recrystallization happened in the cold severe plastic deformation. The strengthening is therefore the synergetic effects of grain refinement and stress-induced phase transformation from β to ω-phase.

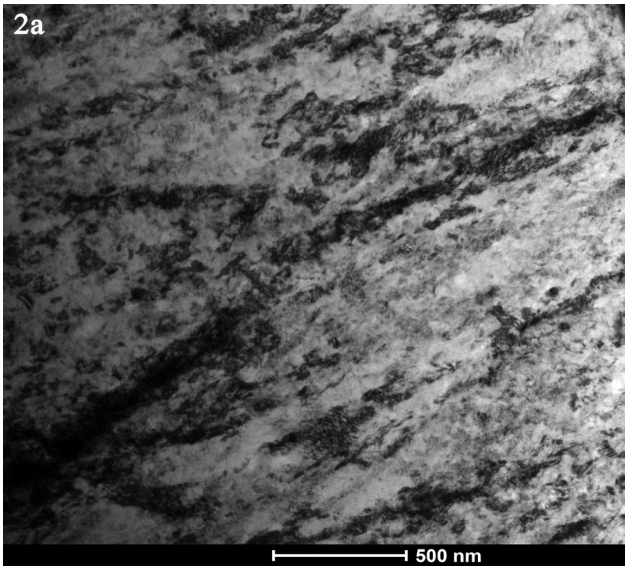

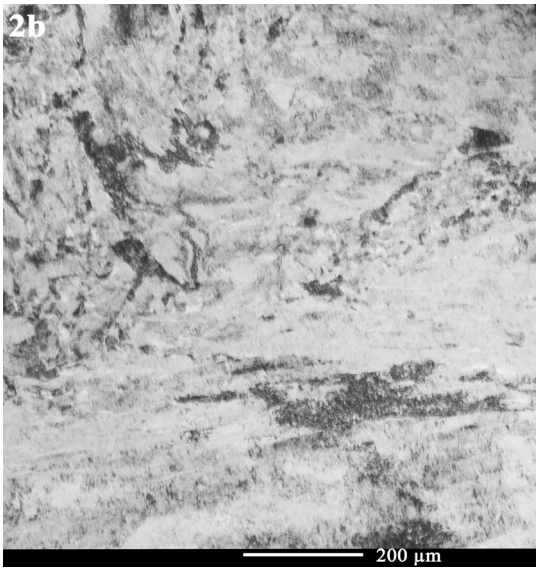

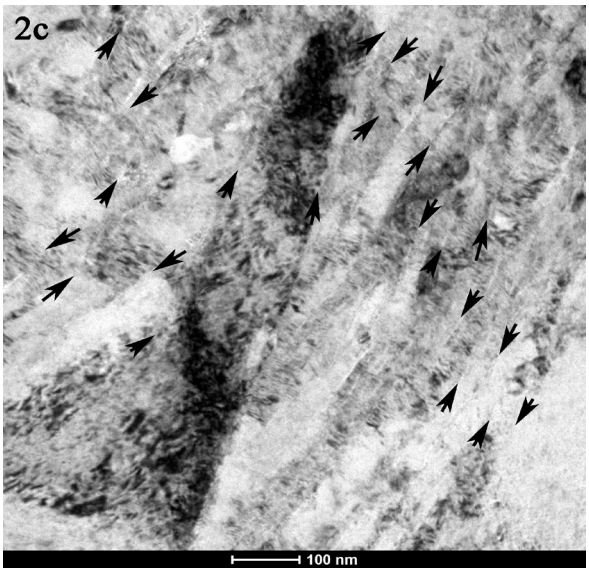

Fig. 2, (a) TEM image of the wire viewed perpendicular to the wire and (b) parallel to the wire and (c) a magnified image showing platelets perpendicular to the wires, arrows indicating platelet boundaries

High resolution TEM images of the severely deformed Ti-15Mo alloy wires revealed a different mode of phase transformation from β to ω under a high strain. From Fig. 3, it is clear that strain induced β to ω phase transformation happened in a planar manor, i.e. through atomic shear of the {2 1 1} planes, resulting in a layered transformation from β to ω in comparison with the athermal ω-phase in the un-deformed rods, which is generally no more than 20 nm in diameter. The transformation still belongs to the diffusion-less athermal phase transformation because no diffusion happens during the phase transformation. However, the additional driving force for the phase transformation is provided as external mechanical energy. The transformation therefore has a strong mark of mechanical deformation of the parental β-phase, i.e. slip on specific planes along specific directions related to the drawing direction. The slip and rotation of the original crystal lattice resulted in the strong planar feature of the ω-phase thus formed. Furthermore, unlike the diffusion controlled isothermal ω-phase, the strain-induced ω-phase does not necessarily have a coherent interface with the matrix β-phase lattice. The high mechanical energy of severe deformation effectively nucleates the ω-phase particles through a cumulative mechanism in a layer-by-layer manner at an atomic level. As a result, ω-phase plates as thin as three atomic layers with a variable size can form in the β-phase matrix, which makes the observation of ω-phase particles in the β-phase matrix difficult. Meanwhile, isothermal ω-phase particles are generally easy to find due to its larger particle sizes [40]. Additionally, due to the near zero stacking fault energy, the transformation can stop or proceed to any intermediate stage between β-phase and α-phase. The low stacking fault energy of β-Ti alloys enables atomic shear in the {2 1 1} planes.

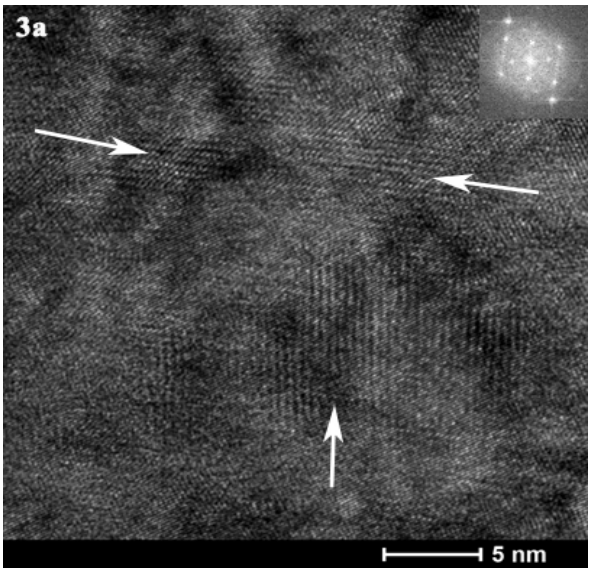
3a
5 nm

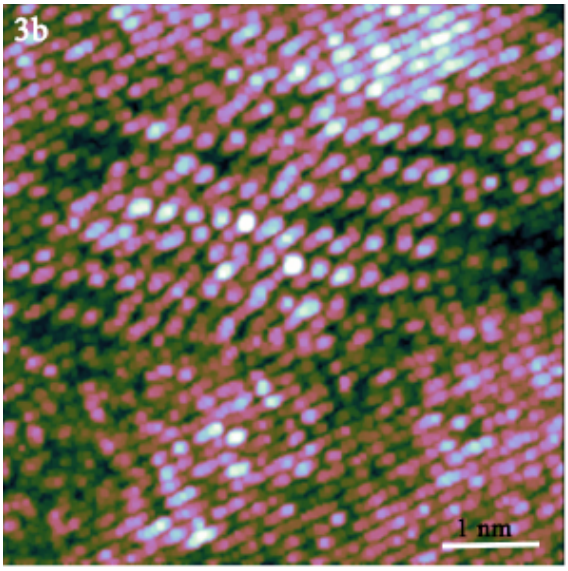
3b
1 nm

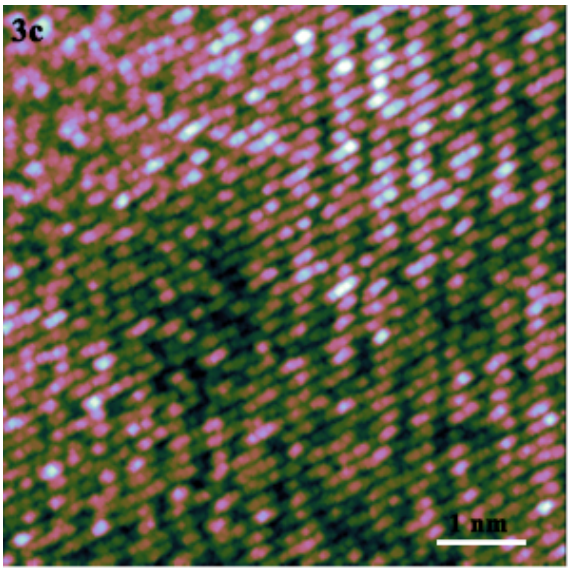

Fig 3, (a) TEM high resolution image of a platelet boundary in Fig. 2 (c) showing atomic shear on the {2 1 1} planes as indicated by arrows and the irregularity of the platelet boundaries (the region between the arrows), (b) an ω particle formed as a result of accumulative shear and (c) a different region of ω phase particle with crystal imperfection

Despite no other phases were observed, homogenization was done at 900^{o}C followed by different quenching rates as described in the Materials and Experiments section to understand the formation of athermal ω-phase. Homogenization at 900^{o}C for 2 hours has eliminated the Mo-depleted particles completely, resulting in a microstructure in Fig. 4 regardless of the cooling rates. Fig. 4 (a) shows modulation and Fig. 4 (b) is a SAD pattern showing no extra crystal features from the modulation. The dark field image in Fig. 4 (c) shows ω-phase particles from the circled ω-phase spots in Fig. 4 (b). These athermal ω-phase particles are the evidence of high stability of the ω-phase in the β-matrix, which has been reported. However, the nature of the modulation is still not clear. It has been reported as twins, composition variation of the β-phase and artifacts, etc. [26, 41] . From the SAD pattern in Fig. 4 (b), it is evidence that there are no other phases than β- and ω-phases. The uniform dispersion of ω-phase particles in the β-matrix is clear. These particles are athermal ω-phase.

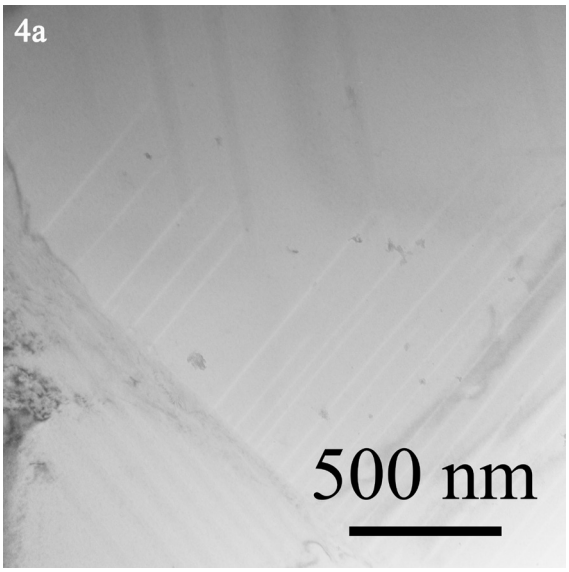
4a
500 nm

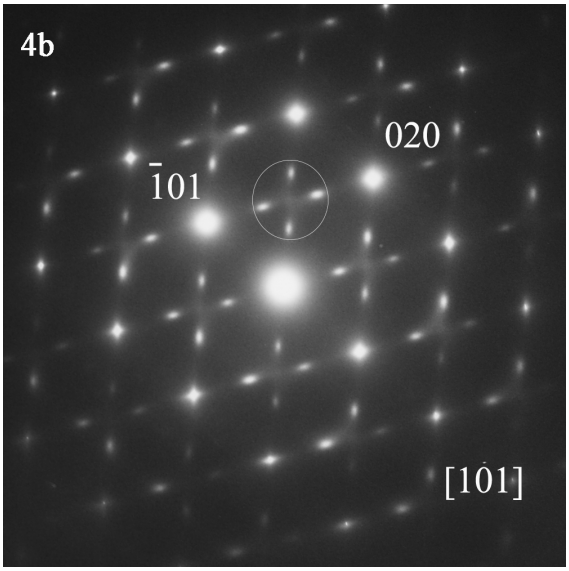
4b
020
$\bar{1}01$
[$\bar{1}01$]

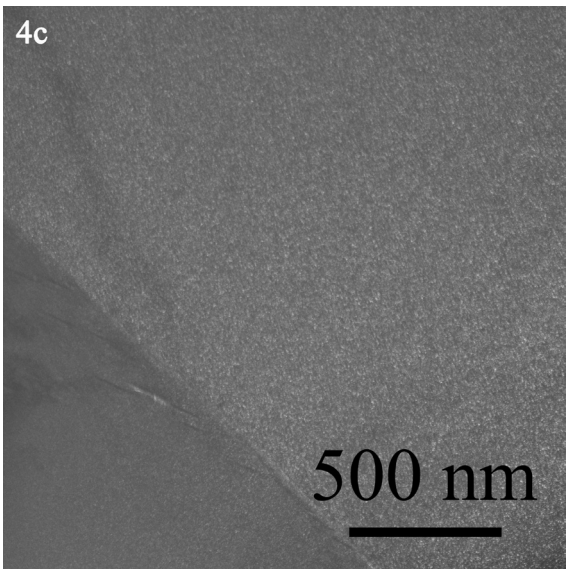

Fig. 4, (a) TEM bright field image of heat-treated sample showing modulation and its corresponding SAD pattern and dark field image showing the uniform distribution of thermal ω particles

Both homogenization at 740^{O}C and 900^{O}C followed by quenching to room temperature have resulted in the formation of athermal ω-phase particles in a β-matrix regardless of the cooling rates. The ω-phase particles are dispersed uniformly in the β-matrix, evidencing a homogeneous nucleation of the ω-phase and a thermodynamic driving force for the β to ω phase transformation. However, the transformation proceeded to a certain level before stopping, suggesting a limitation for the thermodynamic driving force, i.e. additional driving force is required for further progress toward ω phase and even more stable α phase from the parental β phase. As reported by others, coarsening of the ω-phase particles can happen in follow on isothermal heat treatment, evidence of the requirement of additional driving force for further β- to ω-phase transformation. The effects of cold working is therefore interesting to explore further.

Two kinds of ω-phases have been reported as isothermal and athermal according to the nature of the phase transformation. Isothermal ω-phase is the product of isothermal annealing to allow sufficient diffusion of alloying elements to form a hexagonal ω-phase structure from a BCC crystal structure of the β-phase. Meanwhile, athermal ω-phase forms as a result of martensitic phase transformation from β-phase, i.e. displaced shuffle, in which two neighboring {2 1 1} atom layers form a middle layer for each three layers [30]. The ω-phase in the rods is a result of athermal

quenching from the β-phase at high temperature, as shown in Fig. 4 (a)-(c). The ω-phase exists as particles dispersed uniformly in the β matrix. A distinctive feature after severe cold deformation is slip bands at an atomic level as shown in Fig. 4 (a) and (b). The bands are, in fact, the results of the shuffling of {2 1 1} planes of the BCC β-phase to transform to ω phase. The phase transformation is resulted from shearing on the {2 1 1} planes due mainly to the near zero stacking fault energy of the {2 1 1} planes. Therefore, the movement of the {2 1 1} planes is a free motion without considering the restraints of the neighboring grains. As a result, a high strain is accumulated in the grain boundaries resulting in the phase transformation further towards stable α phase.

Conclusions

β to ω phase transformation in a Ti15Mo alloy is characterized by an athermal transformation in heat treatment, which is followed by an atomic strain induced transformation in cold working. The transformation is accomplished through the accumulative shear of {2 1 1} planes. The β to ω phase transformation is not a single step process directly from β to ω but experiencing a continuous rotation of the {2 1 1} planes. The strain induced phase transformation through shuffling of crystal planes of zero stacking fault energy inevitably results in the presence of intermediate crystal structures between the β and ω phases.

Acknowledgement

X.W. would like to acknowledge Medtronic Inc. for the financial support of the research.

References

1. Geetha, M., et al., *Ti based biomaterials, the ultimate choice for orthopaedic implants–a review.* Progress in materials science, 2009. **54**(3): p. 397-425.

2. Gonzalez, J. and J. Mirza-Rosca, *Study of the corrosion behavior of titanium and some of its alloys for biomedical and dental implant applications.* Journal of Electroanalytical Chemistry, 1999. **471**(2): p. 109-115.

3. Burstone, C.J. and A.J. Goldberg, *Beta titanium: a new orthodontic alloy.* American journal of orthodontics, 1980. **77**(2): p. 121-132.

4. Qazi, J., H. Rack, and B. Marquardt, *High-strength metastable beta-titanium alloys for biomedical applications.* JOM Journal of the Minerals, Metals and Materials Society, 2004. **56**(11): p. 49-51.

5. Rack, H. and J. Qazi, *Titanium alloys for biomedical applications.* Materials Science and Engineering: C, 2006. **26**(8): p. 1269-1277.

6. Wang, K., *The use of titanium for medical applications in the USA.* Materials Science and Engineering: A, 1996. **213**(1-2): p. 134-137.

7. Bania, P.J., *Beta titanium alloys and their role in the titanium industry.* JOM Journal of the Minerals, Metals and Materials Society, 1994. **46**(7): p. 16-19.

8. Boyer, R. and R. Briggs, *The use of β titanium alloys in the aerospace industry.* Journal of Materials Engineering and Performance, 2005. **14**(6): p. 681-685.

9. Boyer, R.R., *New titanium applications on the Boeing 777 airplane.* Jom, 1992. **44**(5): p. 23-25.

10. Boyer, R.R., *Aerospace applications of beta titanium alloys.* JOM Journal of the Minerals, Metals and Materials Society, 1994. **46**(7): p. 20-23.

11. Dalmau, A., et al., *Electrochemical behavior of near-beta titanium biomedical alloys in phosphate buffer saline solution.* Materials Science and Engineering: C, 2015. **48**: p. 55-62.

12. Schutz, R., *Environmental behavior of beta titanium alloys.* JOM Journal of the Minerals, Metals and Materials Society, 1994. **46**(7): p. 24-29.

13. Ahmed, M., et al., *The evolution of microstructure and mechanical properties of Ti–5Al–5Mo–5V–2Cr–1Fe during ageing.* Journal of Alloys and Compounds, 2015. **629**: p. 260-273.

14. Kuroda, D., et al., *Design and mechanical properties of new β type titanium alloys for implant materials.* Materials Science and Engineering: A, 1998. **243**(1): p. 244-249.

15. Laheurte, P., et al., *Mechanical properties of low modulus β titanium alloys designed from the electronic approach.* Journal of the mechanical behavior of biomedical materials, 2010. **3**(8): p. 565-573.

16. Niinomi, M., T. Akahori, and M. Nakai, *In situ X-ray analysis of mechanism of nonlinear super elastic behavior of Ti–Nb–Ta–Zr system beta-type titanium alloy for biomedical applications.* Materials Science and Engineering: C, 2008. **28**(3): p. 406-413.

17. Xie, K.Y., et al., *Nanocrystalline β-Ti alloy with high hardness, low Young's modulus and excellent in vitro biocompatibility for biomedical applications.* Materials Science and Engineering: C, 2013. **33**(6): p. 3530-3536.

18. Zhang, J., et al., *Complexion-mediated martensitic phase transformation in Titanium.* Nature Communications, 2017. **8**: p. 14210.

19. Duerig, T., et al., *Formation and reversion of stress induced martensite in Ti-10V-2Fe-3Al.* Acta Metallurgica, 1982. **30**(12): p. 2161-2172.

20. Furuhara, T., T. Maki, and T. Makino, *Microstructure control by thermomechanical processing in β-Ti–15–3 alloy.* Journal of Materials Processing Technology, 2001. **117**(3): p. 318-323.

21. Jones, D.R., et al., *The α–ω phase transition in shock-loaded titanium.* Journal of Applied Physics, 2017. **122**(4): p. 045902.

22. Marteleur, M., et al., *On the design of new β-metastable titanium alloys with improved work hardening rate thanks to simultaneous TRIP and TWIP effects.* Scripta Materialia, 2012. **66**(10): p. 749-752.

23. Nag, S., et al., *Novel mixed-mode phase transition involving a composition-dependent displacive component.* Physical review letters, 2011. **106**(24): p. 245701.

24. Williams, J., D. De Fontaine, and N. Paton, *The ω-phase as an example of an unusual shear transformation.* Metallurgical Transactions, 1973. **4**(12): p. 2701-2708.

25. Zhan, H., et al., *On the deformation mechanisms and strain rate sensitivity of a metastable β Ti–Nb alloy.* Scripta Materialia, 2015. **107**: p. 34-37.

26. Fan, J., et al., *The origin of striation in the metastable β phase of titanium alloys observed by transmission electron microscopy.* Journal of applied crystallography, 2017. **50**(3).

27. Laheurte, P., A. Eberhardt, and M.-J. Philippe, *Influence of the microstructure on the pseudoelasticity of a metastable beta titanium alloy.* Materials Science and Engineering: A, 2005. **396**(1): p. 223-230.

28. Lai, M., et al., *Origin of shear induced β to ω transition in Ti–Nb-based alloys.* Acta Materialia, 2015. **92**: p. 55-63.

29. Salib, M., et al., *Influence of transformation temperature on microtexture formation associated with α precipitation at β grain boundaries in a β metastable titanium alloy.* Acta Materialia, 2013. **61**(10): p. 3758-3768.

30. Zheng, Y., et al., *The effect of alloy composition on instabilities in the β phase of titanium alloys.* Scripta Materialia, 2016. **116**: p. 49-52.

31. Burgers, W., *On the process of transition of the cubic-body-centered modification into the hexagonal-close-packed modification of zirconium.* Physica, 1934. **1**(7-12): p. 561-586.

32. McQuillan, M., *Phase transformations in titanium and its alloys.* Metallurgical Reviews, 1963. **8**(1): p. 41-104.

33. Ng, H.P., et al., *Phase separation and formation of omega phase in the beta matrix of a Ti–V–Cu alloy.* Acta Materialia, 2011. **59**(8): p. 2981-2991.

34. Williams, J., B. Hickman, and D. Leslie, *The effect of ternary additions on the decompositon of metastable beta-phase titanium alloys*. Metallurgical Transactions, 1971. **2**(2): p. 477-484.

35. Lütjering, G. and J.C. Williams, *Special Properties and Applications of Titanium.* Titanium, 2007: p. 383-415.

36. Sun, F., et al., *The role of stress induced martensite in ductile metastable Beta Ti-alloys showing combined TRIP/TWIP effects.* Materials Today: Proceedings, 2015. **2**: p. S505-S510.

37. Zhang, J., et al., *Microstructural evolution of a ductile metastable β titanium alloy with combined TRIP/TWIP effects.* Journal of Alloys and Compounds, 2017. **699**: p. 775-782.

38. Greeff, C., D. Trinkle, and R. Albers, *Shock-induced α–ω transition in titanium.* Journal of Applied Physics, 2001. **90**(5): p. 2221-2226.

39. Cheng, Z., et al., *Extra strengthening and work hardening in gradient nanotwinned metals.* Science, 2018. **362**(6414): p. eaau1925.

40. Nag, S., R. Banerjee, and H. Fraser, *Microstructural evolution and strengthening mechanisms in Ti–Nb–Zr–Ta, Ti–Mo–Zr–Fe and Ti–15Mo biocompatible alloys.* Materials Science and Engineering: C, 2005. **25**(3): p. 357-362.

41. Spurling, R., A., Rhodes, C., G., and Williams, J., C., Metall. Trans. 5 (1974) 2597-2600.